A Stochastic Hole Trapping-Detrapping Framework for NBTI, TDDS and RTN

Sharang Bhagdikar and Souvik Mahapatra*
Department of Electrical Engineering
Indian Institute of Technology Bombay
Mumbai 400076, India
*Phone: +91-222-572-0408, Email: souvik@ee.iitb.ac.in

***Abstract*--A stochastic framework is presented to model hole trapping and detrapping into and out of individual defects that are present in the gate dielectric of a p-channel MOS transistor. The model calculates thermionic reactions between uncharged and charged states of a defect that are separated by an energy barrier, by using the Gillespie Stochastic Simulation Algorithm (GSSA). The model is validated using experimental data from small area devices under Negative Bias Temperature Instability (NBTI), Random Telegraph Noise (RTN) and Time Dependent Defect Spectroscopy (TDDS) studies.**

***Keywords*—GSSA, NBTI, RTN, TDDS.**

I. INTRODUCTION

NBTI is a key reliability concern in small and large area pMOSFETs [1]. The degradation and recovery of ΔV_T during and after NBTI stress is due to the cumulative contributions from interface trap generation (ΔV_{IT}), hole trapping (ΔV_{HT}) and bulk trap generation (ΔV_{OT}) subcomponents. Accurate modelling of the same requires understanding the physical mechanisms that govern these processes.

Hole trapping and detrapping results in drain current and threshold voltage instabilities during NBTI, RTN and TDDS studies [2]-[4]. Historically, the Shockley-Read-Hall (SRH) mechanism is used to calculate the time kinetics [5], usually with temperature (T) activated capture cross section to account for trap relaxation and phonon coupling effects [6]. Alternatively, trap relaxation effect is handled by using thermionic [7] or non-radiative multi-phonon (NMP) [8] processes, in models that treat the uncharged and charged states of a defect as two energy levels; either separated by an energy barrier [7] or represented as intersecting parabolic potentials of a quantum harmonic oscillator [8]. Deterministic implementation of these models are used for NBTI kinetics in large area devices [9], [10], and the stochastic implementation of the multi-phonon model are used for NBTI and TDDS kinetics in small area devices [11]. Note, the original thermionic model of [7] is modified in [9] using a thermally activated barrier for explanation of NBTI stress-recovery kinetics under different T. This deterministic Activated Barrier Double Well Thermionic (ABDWT) model [9] is further validated in [12] by using NBTI stress-recovery data from diverse experimental conditions (wide stress V_G and T ranges) and different technologies. Moreover, the dependence of capture (τ_c) and emission (τ_e) times, associated with hole trapping and detrapping during TDDS and RTN on gate voltage (V_G) is not shown in [11]. This particular aspect is addressed by the extended multi-phonon model of [4]. However large number of parameters (mean + spread = 22) makes it hard to implement in practical situations. Moreover, explanation of NBTI kinetics (like in [12]) is not shown (yet) even using [4].

II. SCOPE OF THIS WORK

The success of deterministic ABDWT model in explaining measured NBTI stress-recovery kinetics over wide T range (–40ºC to +150ºC) and for multiple technologies, such as Silicon Oxynitride (SiON), Gate First (GF) High-K Metal Gate (HKMG) and Replacement Metal Gate (RMG) HKMG based planar and FinFET devices [9], [12] has motivated the stochastic version of the same in this work. The mean of multiple stress-recovery simulations matches mean NBTI kinetics measured in multiple small area devices under different stress V_G and T. The V_G and T dependence of τ_c and τ_e for RTN and TDDS studies can be explained. The time kinetics of individual defects during TDDS can also be explained.

III. MODEL FRAMEWORK

The ABDWT model provides transition rates for charge (hole in p-FET) capture and emission within a trap, Fig.1. The hole capture reaction is modeled as a transition from a reference neutral state (E_1) to the charged state (E_2) via a barrier (E_B). The barrier E_B and state E_2 reduces when a gate bias (V_G) is applied [12]. The barrier energy E_B is distributed in energy to model the spatial and energetic distribution of traps. For setting up the stochastic simulation, a finite number of defects are randomly distributed at the Si/oxide interface. Each defect is assigned random barrier energy E_B obtained from a normal distribution. Simulations are performed on multiple devices by invoking GSSA [13] to generate individual trapping and detrapping transients. A hole trapping (or detrapping) event manifests onto the stochastic ΔV_{HT} transient as a positive (or negative) discrete jump. Macroscopic simulation with identical ABDWT model parameters [12] is shown to match mean of multiple stochastic simulations.

IV. NBTI VALIDATION

Fig.2 depicts measured ΔV_T stress kinetics from multiple small area devices of type D2 [12] at a reference stress V_{GSTR} and temperature (T) along with their mean. Mean of measured ΔV_T kinetics is modeled by the macroscopic BAT framework [2], which isolates the subcomponents ΔV_{IT} (generation of interface traps) and ΔV_{HT}. It is seen that the impact of ΔV_{HT} is relatively higher at shorter stress time and lower T whereas

978-1-7281-0940-4/19/$31.00 ©2019 IEEE

ΔV_{IT} dominates at long stress time and high T. Mean of individual stochastic ΔV_{HT} traces is shown to converge with the macroscopic model ΔV_{HT}, Fig.3. Comparison of stochastic mean with experimental ΔV_{HT} (mean) is performed for a range of V_{GSTR} (Fig.4) and with macroscopic ΔV_{HT} curves for a range of T (Fig.5) to affirm the veracity of the model in a rigorous fashion. In Figs.6-9, similar treatment is accorded to the ΔV_{HT} transients during recovery: matching of mean and macroscopic (Fig.6), isolating the mean ΔV_{HT} from measured data (Fig.7) using BAT, and model experimental data for various V_G (Fig.8) and T (Fig.9). Fig.10 and 12 depict the measured ΔV_{HT} time kinetics during stress and recovery respectively over an extended temperature range (-40°C to +150°C) for device type D3 [12]. The model calculated time transients are reproduced in Fig.11 and 13 and are shown to be concurrent with experimental data over the large temperature range.

V. RTN AND TDDS VALIDATION

Fig.14 shows dependence of τ_c and τ_e on V_G obtained from RTN measurements at various T [3]. This is reproduced by model (Fig.15) that reveals similar T activation trends. Correlation of τ_c and τ_e with change in temperature [3] is depicted in Fig.16. A slope greater than 1 indicates τ_e is more strongly coupled with T whereas a slope less than 1 suggests a stronger coupling for τ_c. For slopes ~1, τ_c and τ_e show equal T acceleration. These trends are modeled in Fig.17 by simulating individual traps with appropriate ABDWT model parameters to generate different T accelerations for each.

Recovery step heights versus emission time plot (Fig.18) from TDDS measurement [11] for ΔV_{HT} dominated (shorter time of stress and lower T) and ΔV_{IT} dominated (longer time of stress and higher T) kinetics is reproduced (Fig.19). ΔV_{HT} dominated kinetics show shorter emission times and hence recover faster. Step heights generated from the stochastic model (Fig.19) are found to be consistent with above.

Fig.20 models the V_G dependence of τ_c and τ_e acquired from TDDS measurements for a non-switching trap [4]. The bias dependence is reproduced across two different T using suitable model parameters for the trap. The vanilla ABDWT model is unable to reproduce the distinct tapering off of capture time constants towards saturation at higher biases, as illustrated in Fig.20. This is addressed by modifying the field activated barrier lowering by introducing a weakly quadratic dependent term in addition to the linearly dependent term which is present in the original model. The same is depicted schematically in Fig.21. The modified ABDWT model yields the correct capture time bias dependence, Fig.22. Prediction of switching trap [4] time constants is also shown using the modified ABDWT model, Fig.23. Prediction of experimental TDDS data of trap 'A1' is performed using the classical NMP transition rates in [14]. These require a correction factor to accurately model the data. In Fig.24, ABDWT is invoked to model the TDDS data of trap 'A1'.

Fig.25 enumerates the distinct types of bias couplings observed in RTN data [15]. The different V_G dependencies can be reproduced by the model upon selection of appropriate parameters.

V. CONCLUSION

GSSA is used to implement stochastic version of the ABDWT model for hole trapping-detrapping. Experimental time kinetics for NBTI stress-recovery are accurately predicted over a range of biases, temperatures and technologies. RTN measured capture-emission time constants are reproduced and their T activation trends are captured Switching and non-switching trap characteristics are modelled using TDDS data. Different V_G dependence of τ_e and τ_c of different RTN traps can be explained.

REFERENCES

[1] S. Ramey, et al, "Intrinsic transistor reliability improvements from 22nm tri-gate technologyv," in *Proc. Int. Rel. Phys. Symp.*, pp. 4C.5.1-4C.5.5, Apr. 2013.

[2] N. Parihar, et al, "BTI Analysis Tool-Modeling of NBTI DC, AC Stress and Recovery Time Kinetics, Nitrogen Impact, and EOL Estimation," in IEEE *Trans. Electron Devices*, vol. 65, no. 2, pp. 392-403, Feb.2018.

[3] H. Miki, et al, "Voltage and temperature dependence of random telegraph noise in highly scaled HKMG ETSOI nFETs and its impact on logic delay uncertainty", in *Symposium on VLSI Technology* (VLSIT), pp. 138, June 2012.

[4] T. Grasser, et al, "On the Microscopic Origin of the Frequency Dependence of Hole Trapping in pMOSFETs", IEDM, Dec. 2012, pp. 19.6.4.

[5] W. Shockley and W. T. Read, Jr., "Statistics of the Recombinations of Holes and Electrons", Phys. Rev. 87, 835, Sep. 1952.

[6] F. Schanovsky, et al, "Advanced modeling of charge trapping at oxide defects", *Simulation of Semiconductor Processes and Devices* (SISPAD), Oct. 2013, pp. 451.

[7] D. Ielmini, et al, "A unified model for permanent and recoverable NBTI based on hole trapping and structure relaxation", 2009 IEEE *International Reliability Physics Symposium*, Apr. 2009, pp. 26.

[8] C. H. Henry and D. V. Lang, "Nonradiative capture and recombination by multiphonon emission in GaAs and GaP", Phys. Rev. B 15, pp. 989, Jan. 1977.

[9] S. Desai, S. Mukhopadhyay, N. Goel, N. Nanaware, B. Jose, K. Joshi and S. Mahapatra, "A comprehensive AC / DC NBTI model: Stress, recovery, frequency, duty cycle and process dependence," 2013 IEEE *International Reliability Physics Symposium* (IRPS), Anaheim, CA, 2013, pp. XT.2.1-XT.2.11. doi: 10.1109/IRPS.2013.6532117.

[10] G Rzepa, et al, "Efficient physical defect model applied to PBTI in high-κ stacks", 2017 IEEE *International Reliability Physics Symposium* (IRPS), pp. XT.11.1-XT.11.6.

[11] Anandkrishnan R, et al, "A Stochastic Modeling Framework for NBTI and TDDS in Small Area p-MOSFETs", *Simulation of Semiconductor Processes and Devices* (SISPAD) , Austin TX, Sep. 2018, pp. 181.

[12] Nilotpal Choudhury, Thirunavukkarasu A, Narendra Parihar, Nilesh Goel and Souvik Mahapatra, "A Semi-Physical Model for Hole Trapping-Detrapping Kinetics During NBTI", IEEE *Trans. Electron Devices* 2019, under review.

[13] Gillespie, Daniel T., "A General Method for Numerically Simulating the Stochastic Time Evolution of Coupled Chemical Reactions", Journal of Computational Physics. 22 (4): 403–434, 1976.

[14] Goes, et al, "Identification of oxide defects in semiconductor devices: A systematic approach linking DFT to rate equations and experimental evidence" *in Microelectronics Reliability* 87, 2018 pp. 286-320.

[15] H. Miki, et al, "Understanding short-term BTI behavior through comprehensive observation of gate-voltage dependence of RTN in highly scaled high-κ / metal-gate pFETs", *Symposium on VLSI Technology* - Digest of Technical Papers, June 2011, pp. 149.

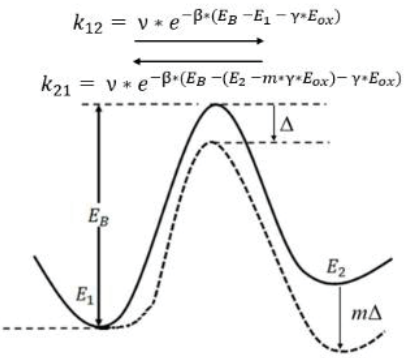

Fig.1. Schematic of ABDWT model. E_1, E_2 and E_b define the energetic configuration of the trap whereas m and γ control the bias coupling.

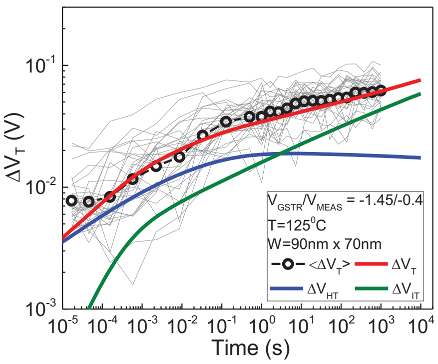

Fig.2. Individual (gray) and mean (black) measured ΔV_T traces during stress along with model calculated mean (red) and decomposition into subcomponents

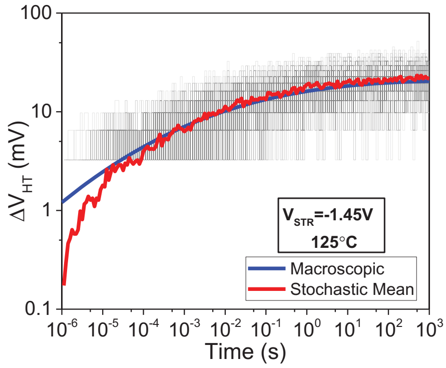

Fig.3. Individual stochastic ΔV_{HT} stress traces (gray) and their mean alongside macroscopic ΔV_{HT} curve.

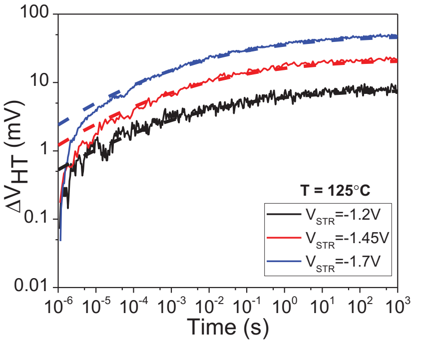

Fig.4. Matching of mean stochastic ΔV_{HT} stress curves (solid lines) with corresponding experimental data (dashed lines) for different stress biases.

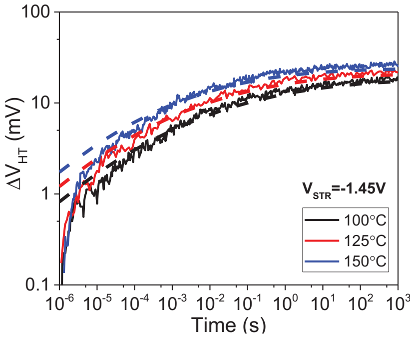

Fig.5. Matching of mean stochastic ΔV_{HT} stress curves (solid lines) with corresponding macroscopic curves (dashed lines) at different temperatures.

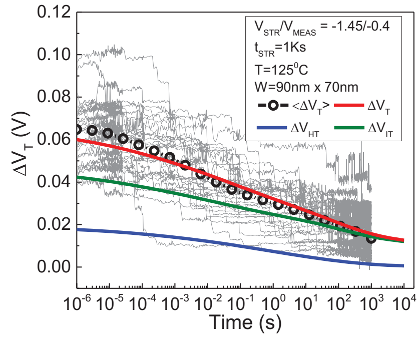

Fig.6. Individual (gray) and mean (black) measured ΔV_T traces during recovery along with model calculated mean (red) and decomposition into subcomponents

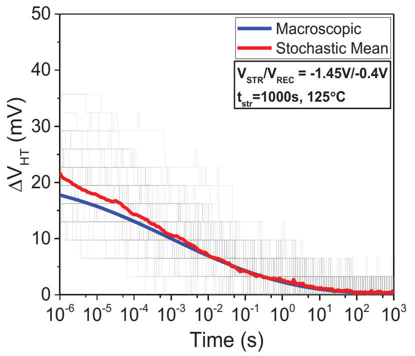

Fig.7. Individual stochastic ΔV_{HT} recovery traces (gray) and their mean alongside macroscopic ΔV_{HT} curve.

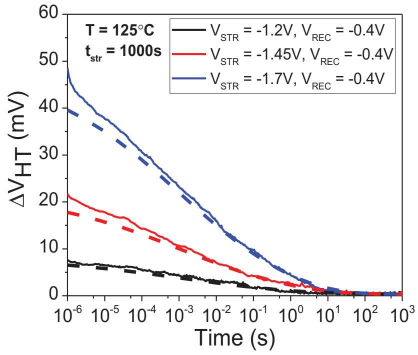

Fig.8. Matching of mean stochastic ΔV_{HT} recovery curves (solid lines) with corresponding experimental data (dashed lines) for different stress biases.

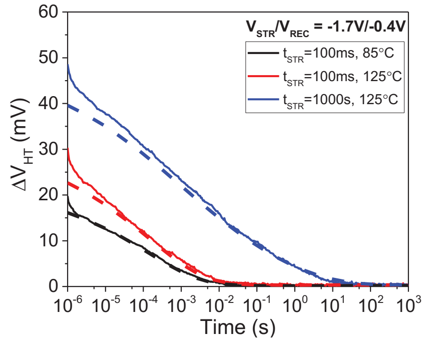

Fig.9. Matching of mean stochastic ΔV_{HT} recovery curves (solid lines) with corresponding experimental data (dashed lines) for different stress time and temperature.

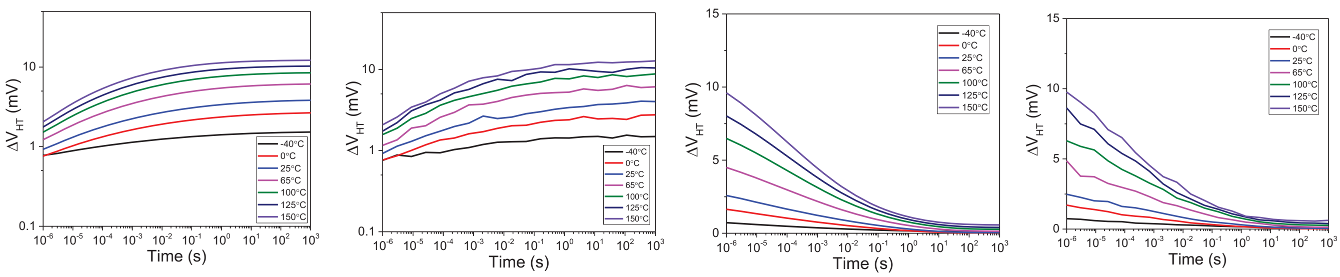

Figs.10-13. Comparison of mean stochastic ΔV_{HT} degradation with experimental data over extended temperature range. Stress and recovery curves are generated and shown to be consistent with measured data. Device is type D3 (RMG HKMG SOI FinFET).

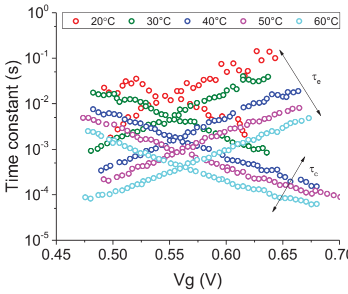

Fig.14. Time constants as a function of V_G at various temperatures from RTN experiments [3].

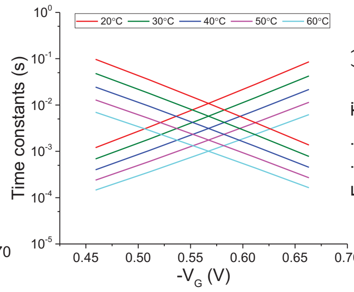

Fig.15. Simulated time constants as a function of V_G at various temperatures.

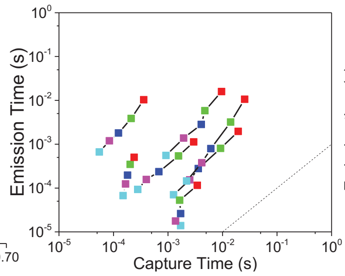

Fig.16. Time constant traces with change in temperature from RTN experiments [3].

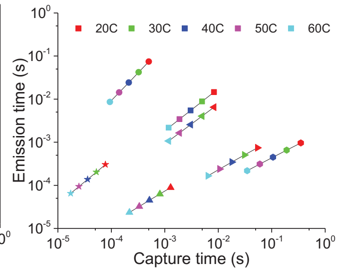

Fig.17. Simulated time constant traces with change in temperature. By suitably choosing model parameters, a wide range of slopes may be obtained.

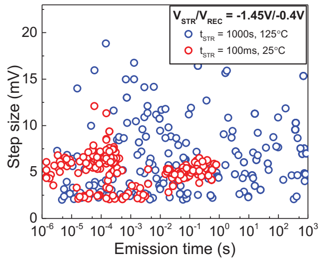

Fig.18. Measured ΔV_T step height versus emission time from TDDS recovery traces.

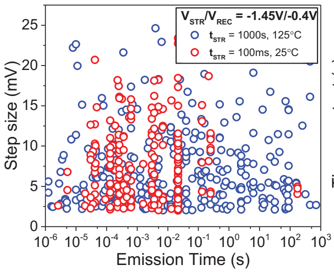

Fig.19. Simulated step height versus emission time generated from stochastic ΔV_{HT} recovery traces.

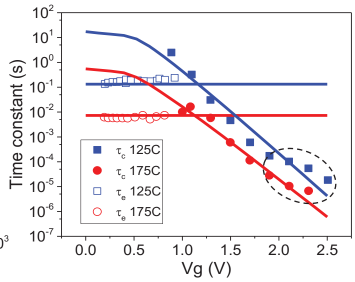

Fig.20. Comparison of TDDS data for non-switching trap [4] (symbols) with model calculated time constants (lines). Model calculation predicts linearly decreasing capture time constant whereas experimental results show tapering off towards saturation at higher biases.

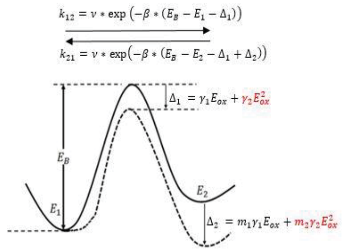

Fig.21. Modified ABDWT schematic diagram. At low biases barrier lowering is linear in Eox while at higher biases it becomes quadratic in Eox.

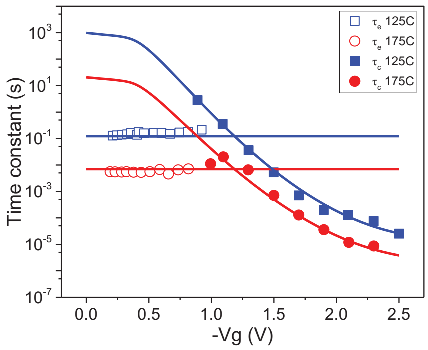

Fig.22. Simulated capture times using the modified ABDWT correctly predicts the tapering off of time constants at higher biases.

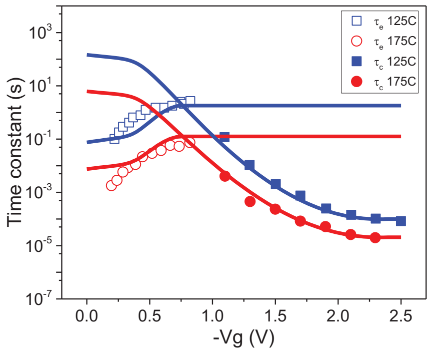

Fig.23. Prediction of TDDS capture and emission time constants (symbols) for switching trap [4] using modified ABDWT (lines).

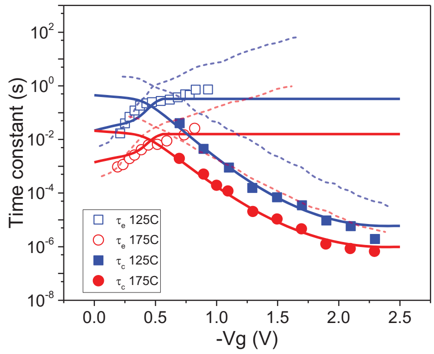

Fig.24. Comparison of TDDS data for trap 'A1' [14] (symbols) with ABDWT model calculated time constants (solid lines) as well as NMP calculated time constants (dashed lines).

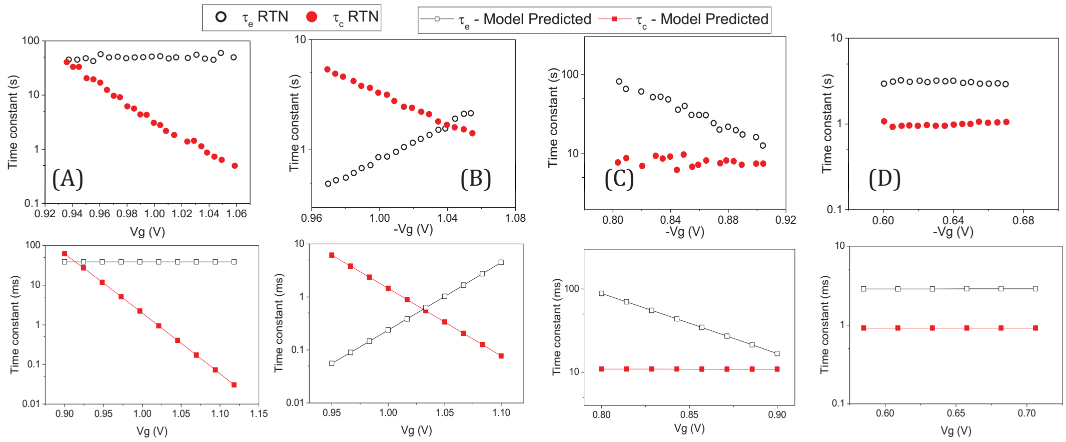

Fig.25. Upper panel depicts various couplings of time constants to V_G extracted from RTN data [15]. (A) $\tau_c < 0$, $\tau_e \sim 0$, (B) $\tau_c < 0$, $\tau_e > 0$, (C) $\tau_c \sim 0$, $\tau_e < 0$, (D) $\tau_c \sim 0$, $\tau_e \sim 0$. Lower panel shows time constants extracted from ABDWT model simulation. Suitable selection of ABDWT model parameters m and γ yields the corresponding bias couplings: (A) $m \sim 1$, (B) $m > 1$, (C) $m < 0$ with small γ, (D) $m \sim 1$ with small γ.